R-38102

19353

PROCEEDINGS REPRINT

SPIE—The International Society for Optical Engineering

Reprinted from

Smart Structures and Materials 1995

Industrial and Commercial Applications of Smart Structures Technologies

2–3 March 1995
San Diego, California

SPIE P PROCEEDINGS SERIES

Volume 2447

©1995 by the Society of Photo-Optical Instrumentation Engineers
Box 10, Bellingham, Washington 98227 USA. Telephone 360/676-3290.

Health error prediction and sensor topology optimization on a smart pressure vessel

Proto R. Factory

Materials Science and Technology Division
Mechanics of Materials Branch, Code 6380
Naval Research Laboratory
Washington DC

ABSTRACT

NRL's Mechanics of Materials Branch has developed a technology that facilitates sensor selection and placement within a composite structure. The Embedded Sensors for Smart Structures Simulator (ES^4) is a tool that relates the output of a finite number of sensors to strain induced structural and material damage. This tool is based on the use of the dissipative part of the bulk nonlinear material behavior. The methodology used to identify this behavior will be briefly described in the present paper. This paper describes the role of strain measurements and their relation to sensor type and location, the conceptual framework of dissipated energy density as the metric employed for assessing material/structure performance. Emphasis is given on the utilization of dissipated energy density for estimating the error between the health of the structure as "seen" by the sensors and the actual health of the structure. Useful applications of this difference are sensor placement optimization in the case of the design phase and confidence level measure for the case of an on board simulating capability.

Keywords: smart structures, smart materials, composite materials, dissipated energy density, sensor error prediction

1. INTRODUCTION

Current research on "Smart" or "Active" materials and structures, in most cases, associates material and structural health with strains or a derivative quantity. This paper along with our recent work on this field[1,2] promotes the use of Dissipated Energy Density as a necessary argument to any material/structure health function. The established methodology can help making decisions concerning the required number of sensors, their type and placement, as well as material and structural health monitoring schemes with emphasis on sensor placement and health error predictions.

The method for the derivation and the usage of dissipated energy density function for a material system makes the following assumptions:

- The composite material system used for the structure has been identified according to NRL's method of extracting the nonlinear material behavior of the system, as captured in the form of the dissipated energy density function [3-5].
- Sensor transfer functions (forward and inverse), and calibration data are available.
- The structural loading rates lie within a range over which the dissipated energy density function for the material is deemed constant for a given loading level.
- The loading condition applied on the structure at any instance, can be always reconstructed as a linear combination of a given and perhaps large set of basis loading cases.

Some of these assumptions affect the use of dissipated energy density based methodology for assessing health, and some affect the process of evaluating the global strain field from the sensor outputs. The method has been applied so far only to organic matrix composites.

The overall strategy followed was motivated by a need to perform the following activities:

- Sensor Network Selection: The selection of sensor type and layout topology.
- Sensor Network Calibration: The calibration of installed sensors.
- Loading Event Simulation: Providing a capability to predict equivalent structural loading from sensor outputs.
- Sensor error prediction.

Realization of these goals, involves resolving a number of technical issues.

Associated with the sensor utilization scheme are these "how to" issues:

- utilize apriori material and structural knowledge
- provide fault tolerance and economic redundancy
- provide independence from structural size and shape considerations
- predict the material state in areas remote from sensor locations
- select an appropriate measure of "Health" which can be defined in terms of sensor output and which provides a spatially and temporally continuous assessment of material state that reflects the degree of material damage
- real time computation capability with reasonable computing resources

To address these issues we have developed an approach that first reconstructs the global structural strain field from the sensor network outputs and from that strain field then predicts the local and global structural health.

2. APPROACH

2.1 Potential scenarios

In general, there are at least two ways to describe the embedded sensors expected functionality. According to the most traditional of these approaches, it is expected that the sensors can only sense the fields of mechanical quantities (i.e. strains, temperature) that excite then in their very close vicinity. In this approach it is also assumed that we know nothing about the mechanical behavior of the structure of interest and about potential loading conditions. As a consequence, sensors have to be placed near the areas of interest (where potential damage may occur). Another consequence of this approach is that the number of required sensors is proportional to the number of locations one is interested to know the material health. This usually leads to a high number of sensors that may in turn start having an effect on the material behavior of the composite. A detailed view of using the sensors of localized health evaluation is shown in Figure 1a.

However, in our case we utilize a second approach that starts with different assumptions about what we know about the structure and the loading conditions. In this case, we utilize all apriori knowledge we have about the structural behavior under certain classes of loading the we are calling "basis loading cases". This enables us to precompute and store on memory of the computing system the strain fields induced on the structure by these loading cases and use them to construct any more complex loading cases from the linear combinations of the basis loading cases. As result we are free from the localized behavior of the sensor. According to this scheme the sensors can be utilized to predict the strain fields vary far away from the area that are placed. This is feasible because in reality it is the whole structure that now behaves like a single distributed sensor whereas the actual sensors serve as "strain matching sites" that help select/construct the right strain field from the precomputed ones. A schematic of this approaches is shown in Figure 1b

2.2. Computation of Sensor Predicted Strains

We assume that the geometric model of the structure can be covered by a mesh of n nodal points as shown in Figure 2.The applied loading at any given moment can be considered a linear combination of r basis loading cases. Figure 2 shows the structure under the influence of the bth basis loading case, where the vertical line signifies the amplitude of strain component u at nodal point i.

The strain field corresponding to the bth basis loading case, L_b is represented by $\varepsilon_{ui}(L_b)$. Where u is the index for strain components and i is the index for the nodal point.and their ranges are given by:

$$\begin{aligned} i &\in \{1, \ldots, n\} \\ u &\in \{1, 2, 3\} \\ b &\in \{1, \ldots, r\} \end{aligned} \tag{1}$$

The strain field induced by an arbitrary loading situation, ε_{ui}, can then be thought of as that resulting from a linear combination of the basis strain fields, $\varepsilon_{ui}(L_b)$, associated with each one of the basis loadings L_b, according to:

$$e_{ui} = \varepsilon_{ui}(L_b)\,\alpha_b. \tag{2}$$

Where α_b are the proportions contributed by individual basis strain fields, $\varepsilon_{ui}(L_b)$.

The basis strain fields $\varepsilon_{ui}(L_b)$ can be computed once via linear elastic finite element analyses and stored for future use. The strains given by equation (2) are the ones that the structure will experience when the corresponding loading is applied to the structure. It is expected that for the general case where grossly asymmetrical sensitivity and/or closeness between basis strain

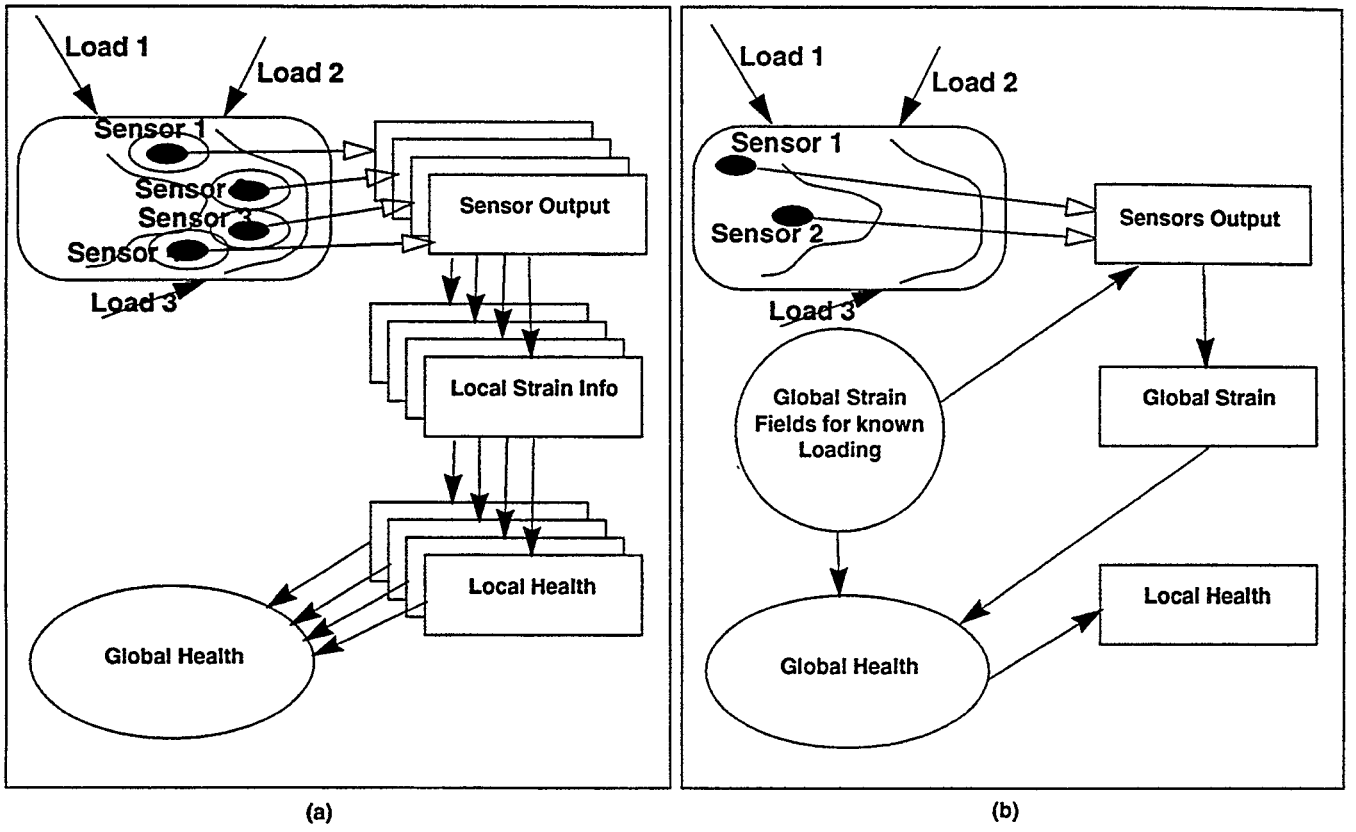

Fig. 1. Localized usage of sensors (a) and distributed usage of sensors (b)

cases exist, the basis will be conditioned by projection into to some acceptable subspace. However, in absence of space we shall skip this step.

By this method the α_b of equation (2) are determined from the sensor outputs.

For the sake of generality we define the sensor output s_k at point k to be a function f_k of a linear combination of the strains at all nodes i, weighted by coefficients a_{kui} according to the expression

$$s_k = f_k(a_{kui} e_{ui}) \quad \text{for} \quad (k \in \{1, \ldots, q\}), \tag{3}$$

where q represents the number of sensors used.

This expression captures both nonlinear and linear sensor model behavior. It is obvious here that the coefficients a_{kui} may play the role of switching on and off the influence of strain components at surrounding nodes, from all to none. Figure 3 shows the sensor output space relative to the geometry of the structure. In this figure the vertical lines signify the amplitude of the sensor output and the small lines on the plane indicate the sensor direction. This provides freedom in orienting the sensors.

We emphasize here that the sensor location need not be at a nodal point. Expression (3) allows interpolation from the surrounding nodal points. An example of such a model is the Extrinsic Fabry-Perot Interferometer (EFPI) optical fiber sensor with a transfer function given by [6]

$$\Delta\phi_k = \frac{4\pi\Delta\lambda}{\lambda_1\lambda_2 L} e_k, \tag{4}$$

where the coefficients a_{kui} are functions of the light sources used (λ_1, λ_2 are the wavelengths of the laser sources used) and geometrical properties of the sensor (L is the gage length of the EFPI sensor). In the optical fiber case it is always assumed that only the local strain components are going to affect them. The role of the sensor output is played by the fringe count dif-

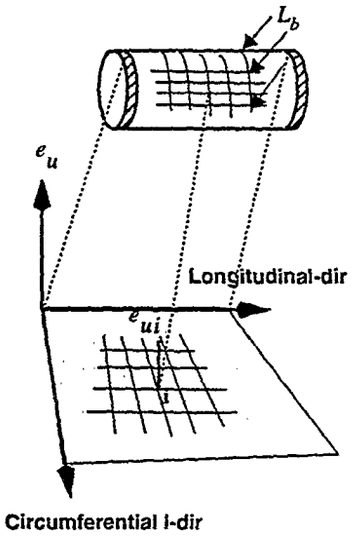

Fig. 2. Strain space associated with the geometry of the structure.

ference $\Delta\phi_k$. In general the coefficients a_{kui} not only reflect influence of the neighborhood, but also contain calibration information for the sensors. The effect of embedding sensors into a material must be determined experimentally. This can be done by weighting the known transfer function of a sensor for the non-embedded case (as in expression (4)), so that the predicted strains will agree with the values measured from an independent and known source such as sets of strain gauges.

Computing strains from sensor outputs requires the inverse g_k, ($g_k = f_k^{-1}$), of the sensor transfer function. Composing both sides of equation (3) with the inverse function f_k^{-1} yields to:

$$f_k^{-1}(s_k) = f_k^{-1}(f_k(a_{kui}e_{ui})), \tag{5}$$

or

$$g_k(s_k) = a_{kui}e_{ui}. \tag{6}$$

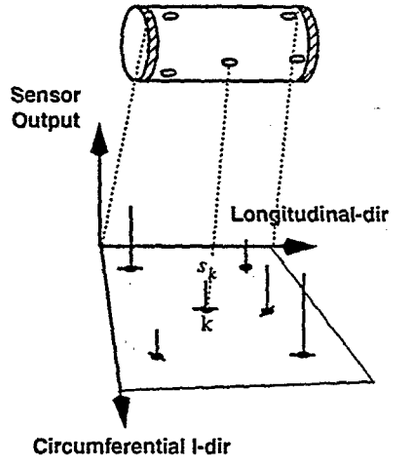

Fig. 3. Sensor output space associated with the geometry of the structure.

Introducing equation (3) into equation (6), we obtain the inverse transfer function depending only on the basis loading case strain fields, i.e.

$$g_k(s_k) = a_{kui}\varepsilon_{ui}(L_b)\,\alpha_b. \tag{7}$$

Provided the pseudo inverse matrix $[a^{kui}e^{b}_{ui}]^P$ exists, the coefficients α_b can be determined uniquely from (7) according to the equation

$$\alpha_b = [a_{kui}\varepsilon_{ui}(L_b)]^P g_k(s_k). \tag{8}$$

We can now compute the predicted nodal strains e'_{ui} by introducing equation (8) into equation (2):

$$e'_{ui} = \varepsilon_{ui}(L_b)\,[a_{kui}\varepsilon_{ui}(L_b)]^P g_k(s_k). \tag{9}$$

The necessary and sufficient conditions for the existence of the pseudoinverse array

$$t_{kb} = [a_{kui}\varepsilon_{ui}(L_b)]^P, \tag{10}$$

is that the number of basis loading cases r be equal to or less than the total number of sensors q i.e.

$$r \le q, \tag{11}$$

and that the array $a_{kui}\varepsilon_{ui}(L_b)$ is non-singular.

To address the problem of using finite computational resources for very high dimensional loading spaces, one employs the approach of utilizing apriori knowledge about the temporal character of loading conditions, to involve lower dimensioned loading subspaces for finite durations.

2.2. Material Health from Dissipated Energy Density

NRL has developed an approach to characterize strain induced material damage [3-7]. This approach was motivated by a need to model failure behavior in composites on a continuum basis and of relating it to material constitutive behavior. The goal of such an approach is to permit accurate modeling of the progressive loss of stiffness and concomitant inelastic behavior.

The procedure involves the determination of an *energy density dissipation function* ϕ that only depends on the strain vector $\underset{\sim}{\varepsilon}$ and the material used in the structure, according to:

$$\phi(\underset{\sim}{\varepsilon}, m) = \phi(\underset{\sim}{\varepsilon}, \underset{\sim}{c}) = c_1(m)\chi_1(\underset{\sim}{\varepsilon}) + \ldots + c_m(m)\chi_n(\underset{\sim}{\varepsilon}) = c_i(m)\chi_i(\underset{\sim}{\varepsilon}), \tag{12}$$

where, $\underset{\sim}{c}$ represents the vector of the material depended coefficients c_i, and χ_i represents the basis functions depending only on strains $\underset{\sim}{\varepsilon}$ and defined at a total of n distinct points distributed over the strain space. Equation (12) can be thought as being an interpolation function allowing evaluation of ϕ on points other than the ones used to define the basis functions.

Its volume integral equals the energy dissipated during loading due to the various internal failure events, and its value at any point in the material is regarded as a measure of load induced internal damage. The energy dissipation function is connected through the total energy offered into the system when loaded and the recoverable energy, through the relationship:

$$\int_0^{u_r} t_u q_v dq^v - \frac{1}{2} t_s u_t u^v = \int_{\partial V} \phi(\varepsilon_i(x_j))\,dx_j \tag{13}$$

The energy density dissipation function thus captures the collective behavior of these failure mechanisms without requiring an explicit knowledge of these mechanisms, and, moreover, can also be related to local stiffness changes which characterize nonlinear structural behavior. The left hand side of equation (13) is known through the automated experimental procedure that involves the In-Plane-Loader (a three degree of freedom robotic testing machine) [3-5].The objective of the In-Plane Loader System (IPLS) is to control the rigid body motion of the boundary of the specimen that is held by the movable grip and at the same time measure the boundary displacements and tractions. Because the actuators are constrained to move in a plane parallel to the specimen, the resulting motion involves only three degrees of freedom relative to any frame of reference on that plane. The left hand side of Equation (13) represents the total energy dissipated due to strain induced damage in the entire specimen.

It is important to note here that the grip motion can be resolved into three basic components: sliding u_x, opening/closing u_y, and rotation ω. Specified combinations of actuator displacements, therefore, map into particular combinations of these three basic motions as shown in Fig. 4(d,e and f).For dimensional homogeneity, u_2 is defined as the length of the arc traveled by a point 1 inch away from the notch tip rigidly connected with the moving grip along the direction of the rotation, instead of using the actual rotation in radians.

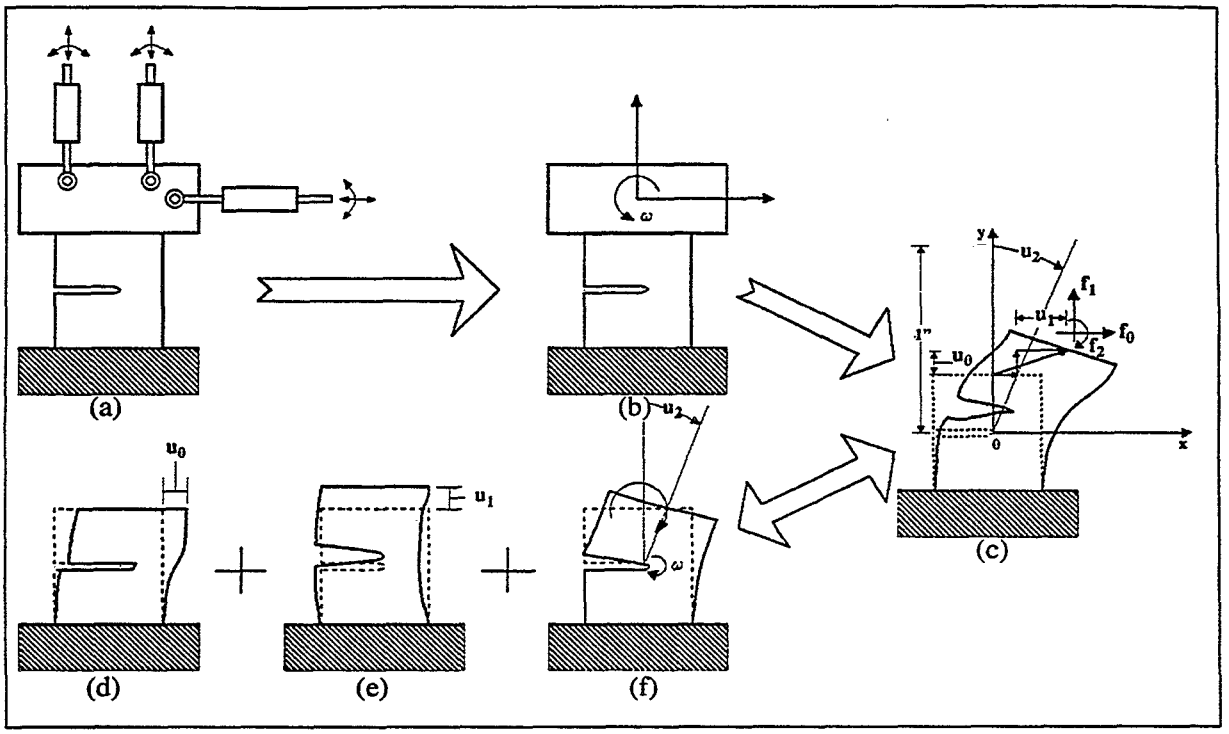

Fig. 4. Schematic of the equivalence between the (a) actuator motions and (b) the three modes of motion , as well as (c) the process of composing an arbitrary loading combination, from linear combinations of the three basic motions: (d) shear, (e) opening/closing and (f) rotation

In order to visualize the loading space it is advantageous to think in terms of a three-dimensional displacement space with coordinates (u_0, u_1, u_2). The issue then is how to select a representative family of paths that cover the space and how to sample along each path. It was decided to cover the boundary displacement space with a set of 15 uniformly distributed radial loading paths as indicated in Fig. 5. Note that because of geometry and material symmetry about the x axis (Fig. 4), only the half-space corresponding to positive sliding displacement (u_0>0) need be considered. The required set of observation points is generated by sampling along each path at 50 distinct points starting from 0 mils and terminating at a maximum of 50 mils of displacement yielding a total of 750 points per material system. Then a particular test in that the actuator motions are continuously varied corresponds to a specific path in this space. This path can be represented by a vector originating from the origin of the space and components given by $u_i = ra_i$ for $i = 0, 1, 2$, where a_i are the coordinates of the unit vectors along the loading path direction, and r is a scalar multiple denoting the proportionality of the path and ranging from 0 to 0.05 inches in steps of 0.001 inches corresponding to the successive observation points. Only 15 specimens are required, and 50 observations per loading path are obtained from a single specimen.

The locus of the end points of all loading paths for the same increment is a half-sphere as shown in Fig. 5, where loading path 11 at an arbitrary increment is presented as an example.The process of computing the total dissipated energy is presented in detail elsewhere[3-6]. The dissipated energy computed this way can be considered to be a measured value since it is derived directly from measured quantities and the only sources of error are from the discrete numerical integration described and the quantization error of the data acquisition process.

After the appropriate number of tests for each material have been performed, the process of determining the dissipated energy density function follows. The construction of this function from a sum of basis functions as shown in Eq. (12) reduces the problem to the determination of the coefficients of these basis functions. This turns out to be a classical optimization problem with inequality constraints where the objective is to minimize the error between the left and the right hand sides of Eq. (12) (objective function). This is a standard problem in quadratic programming and is readily solved using well-established numerical techniques. The computed coefficients are subsequently stored in a data base for the material data. After this step the dissipated energy density is fully defined and given a strain field can be evaluated at any point of any structure made of one of the

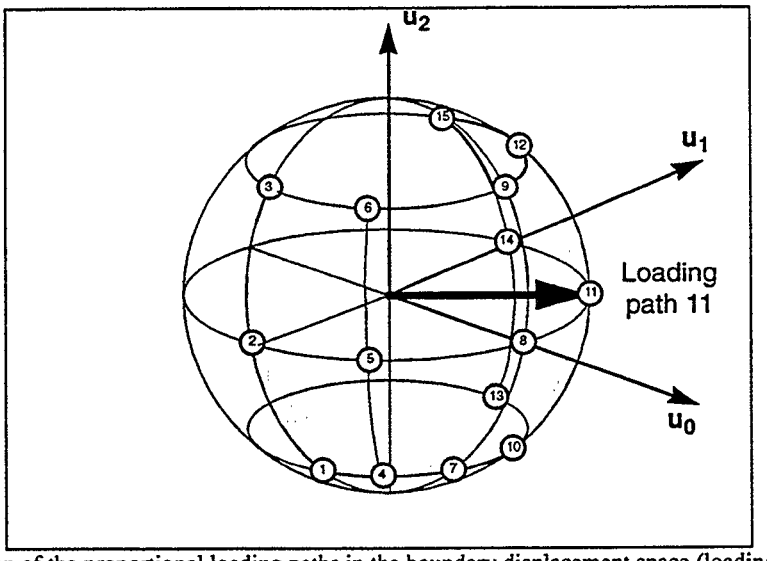

Fig. 5. Definition of the proportional loading paths in the boundary displacement space (loading path 11 is a representative case), and the uniform distribution of the 15 paths used in the present methodology.

characterized materials. This activity is the heart of the simulating technology evolved at NRL for the past 5 years.

In the recent years the dissipated energy density function has been used by NRL not only as a measure of local material softening due to load induced damage, but also as a quantity to describe the non-linear damage response of composite materials as well as the global softening response of composite structures.

It is therefore very natural to consider that since the dissipated energy density effectively provides a measure of damage, that the health of the material can be expressed at any point in the structure as a complementary quantity. One can view a situation, in which the observer of a dissipated energy density contour map on a structure, associates good health of the material at places of low dissipated energy density. The dissipated energy density at every point in the structure can be computed if the strains are known. Computing and plotting the dissipated energy density contour or fringe maps over the entire structure thus becomes a computationally intensive though trivial task.

In the context of the present paper the dissipated energy density can be plotted for the actual strains as computed from the forward analysis for a given loading condition and then from the sensor predicted strains as they are obtained from equation (9). Theoretically if condition (11) is satisfied the comparison between these two maps should show no difference. However, in the case of controlled conditions, a variation between the two images may indicate the need for fine tuning of the calibration coefficients for the selected sensor network. It can also be used to select an alternative sensor system and establish its corresponding calibration in-situ.

2.3. Embedded Sensors for Smart Structures Simulator

To facilitate the process of displaying the dissipated energy density maps in a dynamic fashion, and for a variety of parameters that may be dynamically varied by the user, NRL has initiated the development of the ES^4 system. This system has been designed to assist the user in satisfying the objectives described in the introduction.

The components of the simulator and their function have been described in our previous works[1,2].

The software involved includes both commercial and custom packages, and is currently running in a distributed fashion over NRL's network of NeXT and SGI workstations and a CRAY YMP/EL. However, there is currently an effort for implementing all functionality on custom applications that run on multiple platforms in order to facilitate distribution. Development of a single workstation version of the simulator has also started

3. CASE STUDY AND RESULTS

The selected geometry consists of a cylinder with 8 I-beam stiffening rings that are attached on the internal wall of the cylinder as shown in Fig. 6. Cylinder and stiffeners are made of an AS4/3501-6 25(0)/67(+/-45)/8(90) laminated composite thermoset material. The two semi-spherical end caps are made of steel.

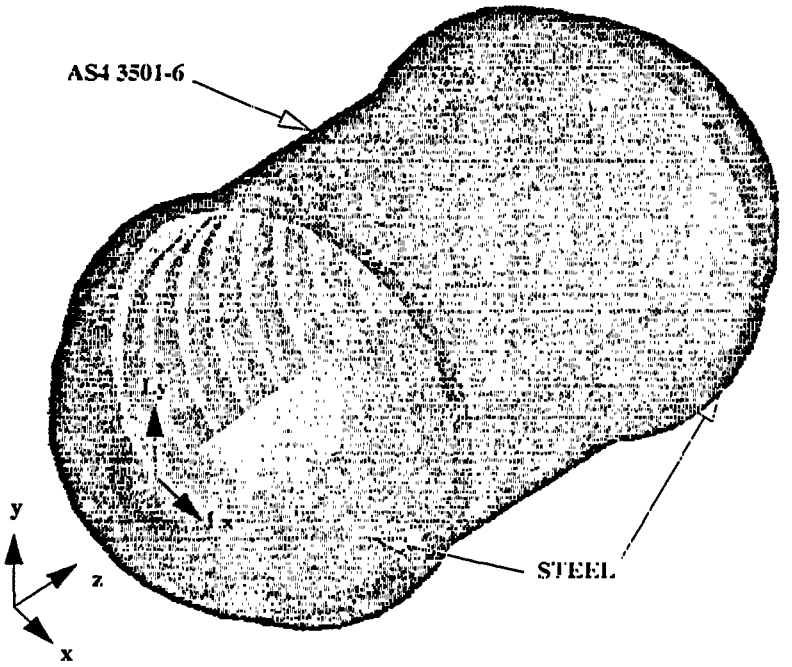

Fig. 6. Geometry, material and loading specification for intersecting cylinders model.

Three basis loading cases were selected. External hydrostatic pressure to capture the effect of depth, and bending about the x-axis and y-axis respectively, in order to capture underwater explosion and maneuvering events. Combinations of these three cases represent a large class of actual loading events. Figure 7 shows a representative dissipated energy density distribution when hydrostatic pressure has been applied on the structure. The strain field has been computed by using ABAQUS 5.2. All nodes of the finite element mesh that lie on the intersection of the upper right end of the cylinder with the end cap have been chosen to be fixed for all six degrees of freedom. The procedure followed to obtain this map was the one indicated by the lower part of Fig. 8 where the concept of computing the error between sensor-predicted and actual health by using the ES^4 simulator is described schematically.

In order to demonstrate the utilization of the diagram shown in Fig. 8, we shall explore the case where the sensors have been "trained" to "see" strain fields caused by linear combinations of only two of the basis loading cases namely pressure and bending about the y-axis (lateral point loading on the tip of the free end cap along the x-axis), while an actual load that includes a component of bending about the x-axis (lateral point loading on the tip of the free end cap along the y-axis), is applied on the structure. Here, "trained" means that the procedure of computing the array given in Eq. (10) has been applied for r=q=2 (which means that only two sensors are needed and that the basis loading cases are actually two as well).

Figure 9 shows the loading space spanned by the three basis loading cases. The labels for the loading cases in figure 8 have been chosen to indicate the participation of the three basis cases with "+" or "-" depending on the sense, and the absence with "0".

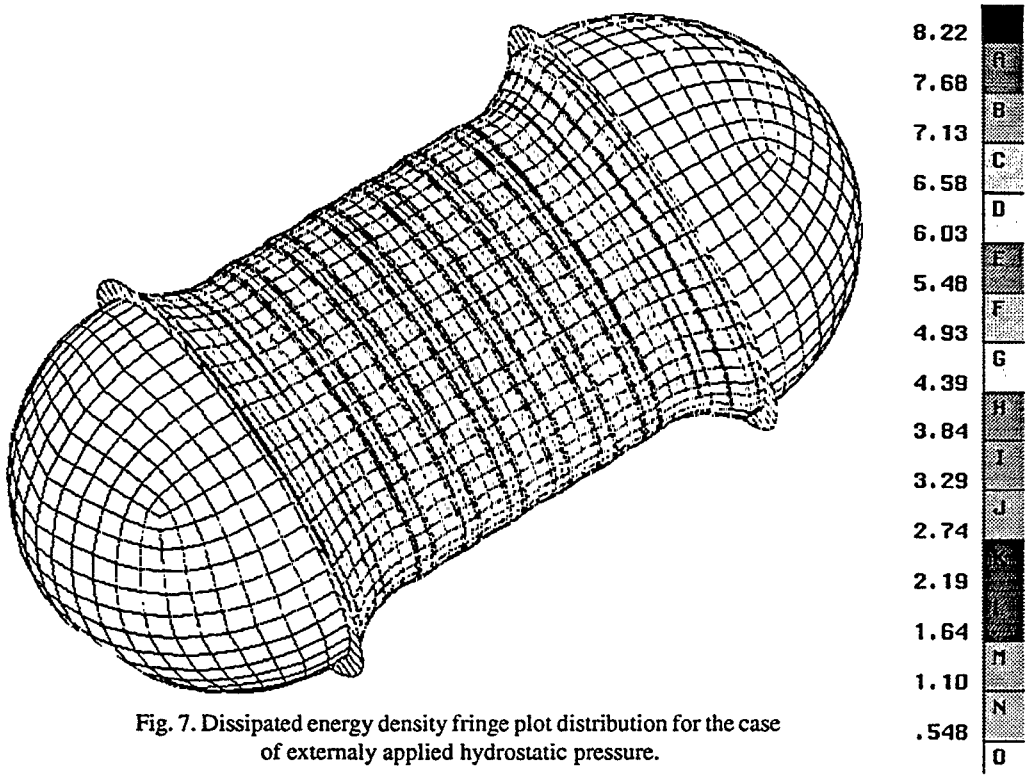

Fig. 7. Dissipated energy density fringe plot distribution for the case of externaly applied hydrostatic pressure.

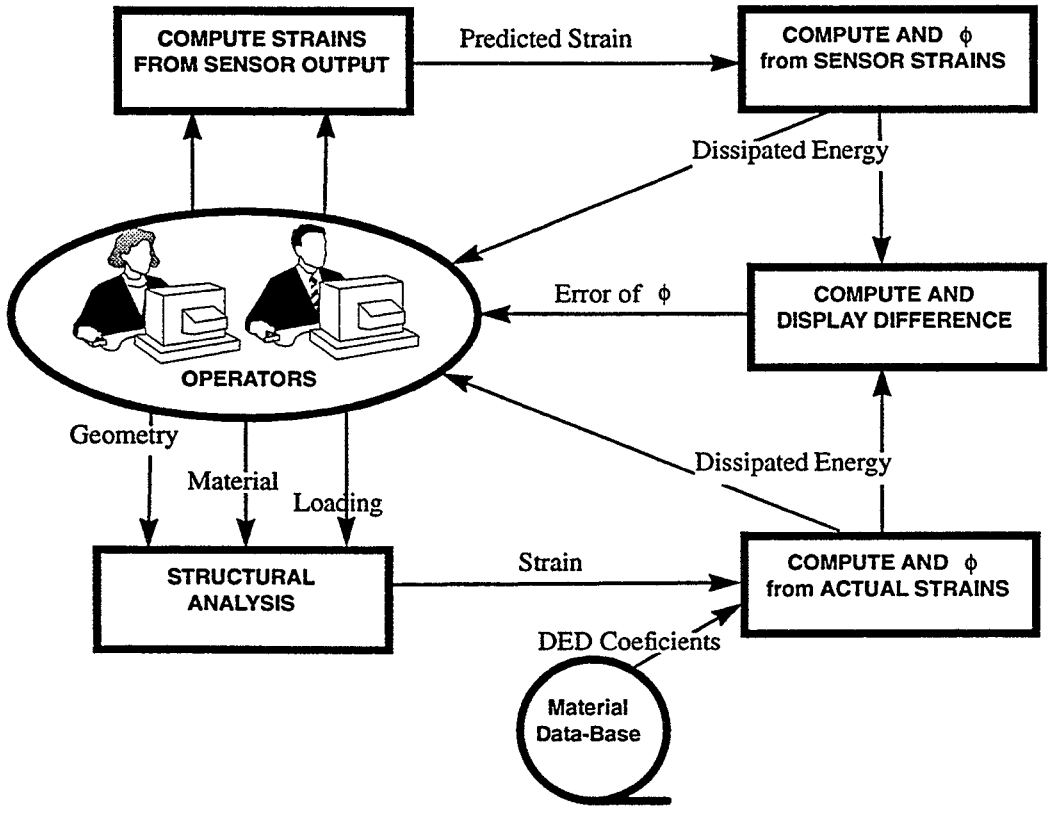

Fig. 8. Computation of error between sensor-predicted and actual health by the use of the ES^4 tool.

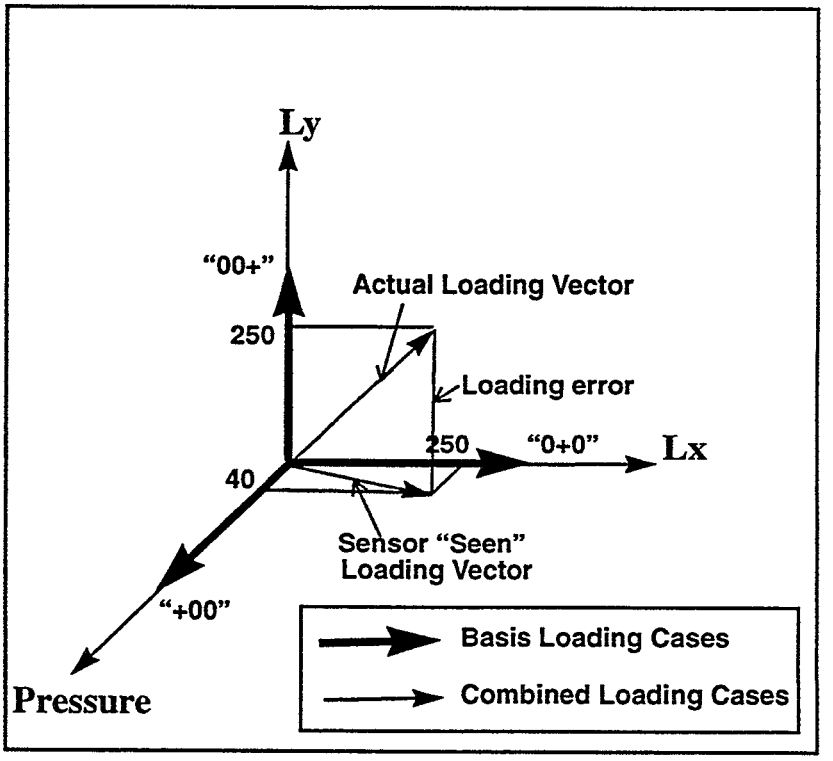

Fig. 9. Basis and combined loading paths embedded in the loading space.

The first position on the label represents the pressure loading case, the second and the third represent the bending loading about the x- and y-axes respectively. To describe the situation between the actual and the predicted health schematically, we present the loading situation described in the previous paragraph, in the loading space shown in Fig. 9. Thus, "Pressure" and "Lx" are the two loading cases that the sensor methodology described in section 2 is aware of. Therefore, the two or more required sensors can only predict strain fields on the structure that are induced from loading conditions that can only be linear combinations of these two components and always are embedded in the "pressure-Lx" plane. When an actual load that includes a component along the third axis of the loading space (namely the Ly axis) is applied on the structure, the sensors will only "see" the projection of this load vector on the "pressure/Lx" plane. As a consequence, an erroneous prediction of the sensed strain field and accordingly of the dissipated energy density will be generated. An application of this process for an actual loading of 40 psi hydrostatic pressure, 250 lb force along the Lx axis, and 250 lb force along the Ly axis has been employed. By using the ES^4 tools to perform the activities on the upper path of the diagram in figure 6 we computed the dissipated energy density distribution that actually corresponds to a sensed loading vector of 40 psi pressure and 250 lb force along the Lx axis, as shown in Figure 7. Then the actual strain field and dissipated energy density distributions were computed by employing the activities shown in the lower part of Fig. 8

Figure 10 shows the top and bottom view distributions of the errors for the case of the dissipated energy density distribution (a) and the case of the root mean square error of strain (b). The RMS error of strains was used as a function that reduces the tree components of strain to a scalar value that can be used to display the combined differences between actual and sensor-predicted strain fields. Any other function can be used to satisfy additional needs of the ES^4 user. By comparing the distributions of dissipated energy density and RMS strain one can observe that the RMS of strains distribution presents very sharp spatial variations from one level of error to another and extend from 0 to 100% error. On the other hand, the dissipated energy density distribution presents smoother variation of error from one level to another and extends from o to 70% error. It therefore generates a much less dramatic error variation with a lesser critical value that indicates a more forgiving character that of the RMS of strains, when considered as a measure of health.

An interesting outcome of this methodology for sensor usage, is that there are areas that the error is very low regardless of the fact that the actual loading is very different from the one the sensors expect. This constitutes the basis of setting up an optimization scheme that attempts minimization of the distributed error and determines the appropriate values of the sensor topology characterization variables that are introduced through the Eq. (3) via the coefficients a_{kui}. A random hill climb with reversal methodology is being currently under its initial implementation at NRL for optimizing sensor location on the basis of this procedure.

Another use of this methodology involves real time estimation of the error in health prediction (for the case of an on board system deployed in actual composite structures), provided an independent way for establishing the actual loading on the structure is in place.

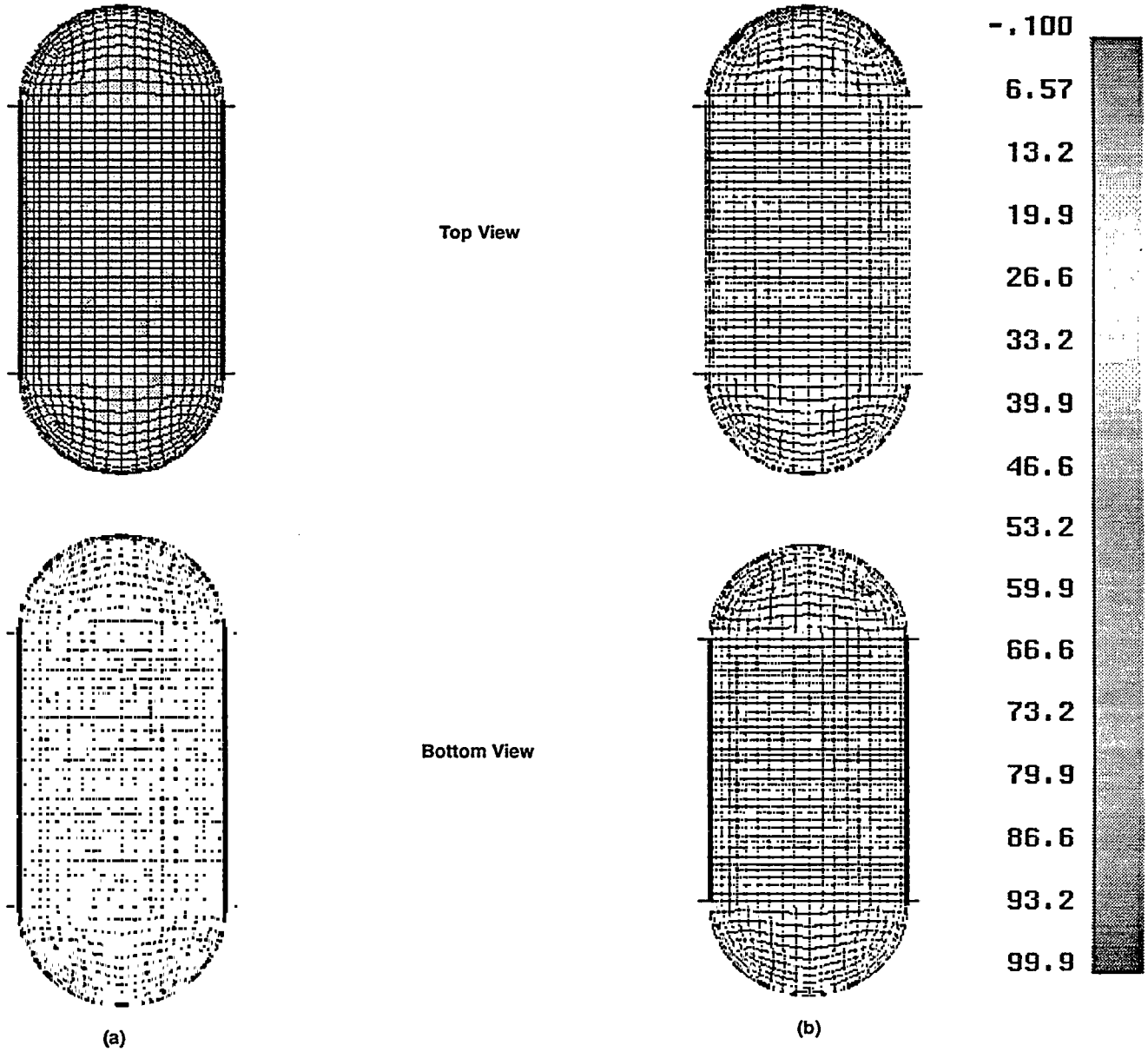

Fig. 10. Top and bottom views of the distributions of dissipated energy density error (a) and the root mean square of strains error (b)

4. DISCUSSION AND CONCLUSIONS

The proposed methodology facilitates the selecting of appropriate sensor types and in their number and placement. Selecting the kind of needed sensors can be a function of many issues that the designer may wish to address. This approach can aid the designer in making decisions about sensor sensitivity and dynamic range.

Selecting the number of required sensors can also be facilitated by our approach. Since it has been established by equation 11 that the number of required sensors has to be at least as large as the number of the expected loading basis cases, the problem has been reduced to deciding the degree of redundancy needed for a specified fault tolerance. A redundant sensor system can be implemented to allow strain prediction recovery in case of sensor fault, partial or total sensor incapacitation. The sensor simulator module provides the designer with the capability of performing "what-if" studies of prediction deterioration as a function of varying degrees of redundancy and varying degrees of sensor incapacitation. Performing sensor network calibration may now be greatly enhanced by virtue of the fact that with appropriate simple experiments the coefficients a_{kui} can be determined in a way which accounts for all of the effects mentioned above, and without specific knowledge of the micromechanical effects. This is done by requiring the sensor detected strains be as close as possible to the actual ones. Through the linear elastic analyses that associate the basis loading cases with the basis strain cases and relations (2) and (9) the loading condition can be reconstructed from the sensor output. Plans exist to extend the structural simulator so as to include a loading event module that can be set to display in terms of actual independent loading events (i.e. underwater depth variation, or depth charge parameter variation).

Prediction of material/structural health depends on the determination of a of a function that maps the dissipated energy density distribution of the smart structure, to the value space of those empowered to say when the structure is or isn't performing its task. We do not pretend to offer this function; only potentially an environment in which it may be determined (i.e. a concept formation laboratory).

Finally, the error between the sensor-predicted health and the actual health of the structure and the material can be generated to provide a measure of confidence of the prediction (especially for on-board installations). It can also be used as an objective function that leads to optimizing the position and the architectural characteristics of the sensor layup.

5. ACKNOWLEDGMENTS

The authors would like to gratefully acknowledge the financial support provided by ARPA under contract no. 6604. We would also like to express our gratitude to Mr. James Kelly for his encouragement and support.

6. REFERENCES

1. J.G. Michopoulos, P.W. Mast, R. Badaliance, I. Wolock, "Health Monitoring of smart structures by the use of dissipated energy", ASME proc. 93 WAM on Adaptive structures and material systems, G.P. Carman/E. Garcia Eds., AD-Vol. 35, pp. 457-462.

2. P. W. Mast, J.G. Michopoulos, R. Badaliance, H. Chaskelis, "Dissipated energy as the means for health monitoring of smart structures", SPIE Proc. Smart Structures and Materials 1994, Smart Sensing, Processing, and Instrumentation, J. Sirkis Ed., Vol. 2191, pp. 199-207.

3. P.W. Mast, G.E. Nash, J.G. Michopoulos, R.W. Thomas, R. Badaliance, and I. Wolock, "Experimental determination of dissipated energy density as a measure of strain-induced damage in composites", Technical Report NRL/FR/6383--92-9369, Naval Research Laboratory, Washington, DC.,1992.

4. P.W. Mast, L.A. Beaubien, M. Clifford, D.R. Mulville, S.A Sutton., R. Thomas, J. Tirosh, and I. Wolock, "A semi-automated in-plane loader for material testing", *Experimental Mechanics*, Vol. 32, pp. 236-241,1983.

5. P.W. Mast, J.G. Michopoulos, R.W. Thomas, R. Badaliance, I. Wolock, "Characterization of strain-induced damage in composites based on the dissipated energy density: Part I,II,III", to appear Int. Jnl. of Theor. and Applied Fract. Mech., 1995

6. Claus, R.O., Gunthor, M.F., Wang, A., and Murphy, K.A., "Extrinsic Fabry-Perot sensor for strain and crack opening displacement measurements from -200 to 900 °C", *Smart Materials and Structures*, Vol. 1, pp. 237-242, 1992.

E-mail Inquiries: factory@ramp1.nrl.navy.mil